

We are IntechOpen, the world's leading publisher of Open Access books Built by scientists, for scientists

6,900

Open access books available

186,000

International authors and editors

200M

Downloads

Our authors are among the

154

Countries delivered to

TOP 1%

most cited scientists

12.2%

Contributors from top 500 universities



WEB OF SCIENCE™

Selection of our books indexed in the Book Citation Index
in Web of Science™ Core Collection (BKCI)

Interested in publishing with us?
Contact book.department@intechopen.com

Numbers displayed above are based on latest data collected.
For more information visit www.intechopen.com



New Trends of Optical Measurements

*Oleg Angelsky, Peter Maksymyak, Claudia Zenkova,
Olexander Ushenko and Jun Zheng*

Abstract

Some of the achievements of modern optical metrology are offered for the reader at this chapter. Optical testing methods have always attracted by their important advantages: distance, non-destructive impact on the test object and, of course, high accuracy. So, using of polarization optics approach, the authors were able to implement the methods for controlling the surface roughness for the moving surface with the measurement accuracy of 10 angstroms. It has become possible to make a breakthrough in the basic methods of measurements from the nano to the femto or pico units of the measured quantity value over the past decades. Control of nano (micro) particle motion by an optical field and their use for testing complex optical fields; ultra-precise determination of the optical parameters of both solid and liquid and gas-like substances by optical methods; by interference methods and many other, are proposed for consideration here. Some biomedical applications are also offered for reader's familiarization. Particularly, the results of 3D Stokes-polarimetric mapping of microscopic biological images with digital holographic reproduction of layer-by-layer ellipticity polarization maps in differential diagnosis of benign and malignant tumors with different degrees of differentiation are presented. The authors have shown that using of polarization-holographic measurements in biomedical applications makes it possible to obtain a reliable diagnostic of pathological states both of biological fluids and solid-state objects.

Keywords: micro- (nano)- object, optical force, spin (orbital) momentum, biological image, interference method, measurement accuracy, measured value, error

1. Introduction

Metrology is a field of scientific and technical research that has absorbed optical engineering and precision measurements, directions that intensively develop.

This is proclaimed by the world achievements in the creation of femtosecond lasers (John L. Hall and Theodor W. Hänsch “for their contributions to the development of laser-based precision spectroscopy, including the optical frequency comb technique”, Nobel Prize in Physics 2005), the making and successful operation of an optical fluorescence microscope with a record resolution of 10 nanometers (Eric Betzig, Stefan W. Hell and William E. Moerner “for the development of super-resolved fluorescence microscopy”, Nobel Prize in Chemistry 2014) [1], and the intensive research in the development and use of optical tweezers, manipulators,

molecular motors, etc. (Arthur Ashkin “for the optical tweezers and their application to biological systems”, Nobel Prize in Physics 2018).

Using the opportunity of optical diagnostics, observation, and measurement, which are opening up thanks to the development of modern methods for the formation of various features of structured light [2], it has become possible to reach the verge of a picometer level resolution of measurements in a practically revolutionary way.

Already today, ways of implementing the measurement of optical field parameters in three-dimensional space [3–5] with nanometer resolution have been outlined. The appropriateness and importance of such measurements are strengthened in the case of study of polarized light transformations and the possibility of realization an ultra-high resolution in the optical range. In this sense, it is necessary to present some biomedical application and to notice the development and experimental testing of a new 3D Stokes-polarimetry method based on mapping of object fields of biological optically anisotropic layers [6, 7]. Here digital holographic layer – by – layer reconstruction of polarization ellipticity distributions is used, e.g. for express diagnosis and differentiation of samples of polycrystalline blood films of patients with prostate tumors [8–10].

The today’s state of physics and life sciences, in general, require expanding the abilities of optical systems by moving from the systems of the so-called millimeter-micrometer range to instruments and devices operating in the nano-, pico-, femto-meter ranges.

The implementation of such tasks is impossible without finding and discovering new technical and technological solutions, the creation of hybrid measurement systems that can simultaneously work in different spectral ranges, using different parameters of the optical radiation field for diagnostics, and evidently their interconnection.

A review of the state of research at this level is based on a platform that has been formed in a number of directions by the authors of this chapter.

So, the goal of this presentation is to analyze new trends of precision measurements in the picometer range, based largely on the results of own research by the authors.

2. Micro and nanostructures and metrology applications

2.1 Using of micro- and nanoparticles for metrology

A new unique tool that has appeared relatively recently and enables optical measurement to be carried out, is a set of methods for capturing, moving, manipulating, controlling of the micro- and nanoparticles motion. To this end, optical traps are created in which optical flows can be controlled using a set of field parameters, namely, amplitude, phase, or polarization.

Thus, various types of traps are formed for spatial capture and movement of nanoscale objects, creating active optical forces of the order of femtonewton [11–13].

Comprehensively considering the methods of creating micro- and nano-manipulators, tweezers and motors, as well as using meye elements, according to our work [11–14], based on classical optical principles, but supplemented with new, and possibly fundamentally new technical and technological solutions for auxiliary devices, new technical problems for optical measurements of micro-, nano - pico femtosecond ranges are solved. Even in the fact that by the speed of microparticles rotation one can determine the absorption coefficient of a matter, the degree of anisotropy of the material, etc. Basically, it can be claimed that these solutions are built on differential, comparative principles and approaches.

2.2 Biaxial crystals in the tasks of creating multifunctional traps for micro- and nano-objects

Based on modern measurement approaches to achieve a nano (femto) units of optical measurements, the possibility for formation of various amplitude-phase, polarization field structures that can be used for manipulating micro- and nano-objects is shown in [12–14]. An interesting solution to this problem is that due to the use of birefringent crystals, it is possible to simultaneously work with various parameters of the optical field, creating a wide arsenal of traps based on one crystal.

Created traps, trapping nanoparticle by an optical field provide determination of nanoparticle parameters with an error of several percent [15].

So the use of birefringent crystals sets the formation of optical fields with deep structure of the inner energy flows. Spread of a slightly divergent (conical) light beam with prescribed linear polarization generates a complicated optical field with spatially inhomogeneous distributions of intensity, phase and polarization that is accompanied by an intricate pattern of the transverse energy flows (**Figure 1**). Here the reader can estimate field distributions at the biaxial crystal output in the vicinity of the optical axis O. Both axes lie in the plane (XZ) so that $x = 0$ corresponds to the middle direction between the axes. The input beam polarization makes an angle 45° with axis X. **Figure 1a** presents both intensity distribution after the output X-oriented polarizer (background) and the transverse orbital flow of the X-polarized component (black arrows). The spin density of the total output field (background), the spin flow map (cyan arrows) and the polarization distribution (gray ellipses) are described in **Figure 1b**.

Such fields offer a variety of possibilities for microparticles' trapping and control, for example:

- a. the intensity minima (maxima) form natural traps for absorbing (dielectric) particles due to the gradient force [16, 17];
- b. phase singularities associated with the amplitude zeros (**Figure 1**) are coupled with the vortex-like orbital flows able to induce rotation of the trapped particle;

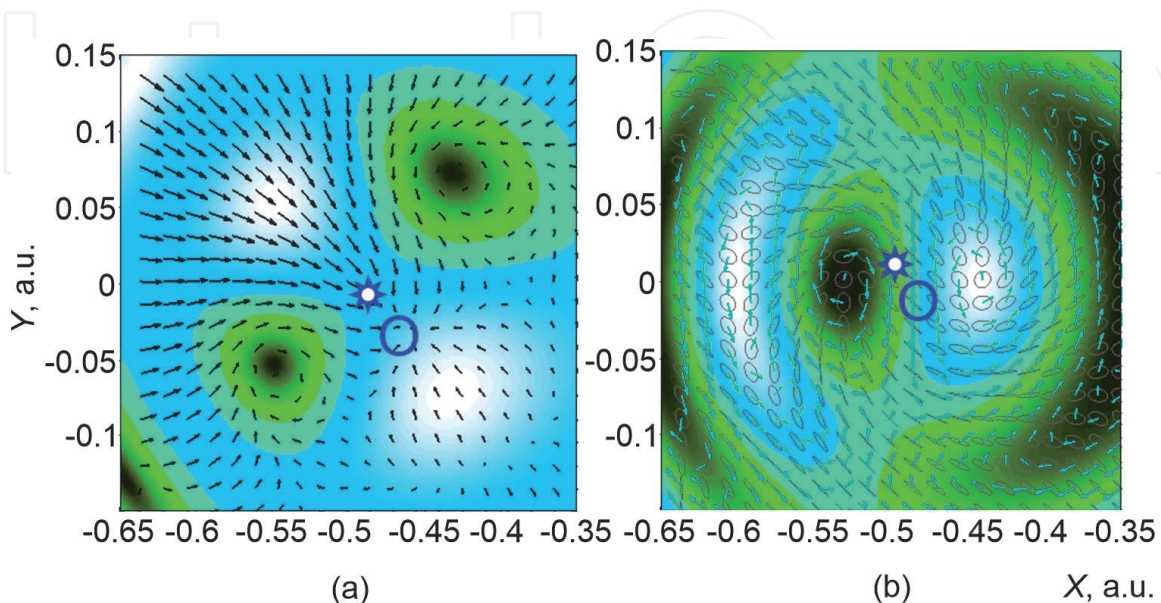


Figure 1.
The scheme of intensity (a), polarization (b) and energy flow (a,b) distribution formed by a birefringent crystal.

- c. both the orbital and spin flows can induce definite motion of particles in the transverse plane (**Figure 1a** and **b**);
- d. the density of spin angular momentum (**Figure 1b**) may induce controllable orbital motion of particles depending on their position within the beam cross section;
- e. the output pattern of optical field distribution can be easily modified via the controllable input and output polarization, providing suitable means for delicate spatial positioning of the trapped particles.

Arrangement of an optical tweezer employing the above principles is shown in **Figure 2**. This optical arrangement based on a birefringent crystal consists from a laser (1) (650 nm, 200 mW), quarter-wave plate – 2, two polarizers – 3, 11, beam expander with spatial filtering – 4, mirror – 5, microobjectives – 6, 8, 13, 17, biaxial crystal with 3D rotating drive – 7, calcite plate – 9, calcite wedges with 2D shifting of one wedge – 10, beam-splitting dichroic cube – 12, sample – 14, white-light source – 15, condenser lenses – 16, CCD-camera – 18, Personal Computer (PC) - 19.

On the other hand, as already noted, the use of nano and micro particles provides a diagnostic tool for optical fields. The optical forces arising in the optical field and acting on these particles are at the nano-, pico- femto- Newton, differing in accordance with the properties, shape and size of the particles. Accordingly, it becomes possible to spatially separate internal optical flows, both with respect to spin and orbitally one.

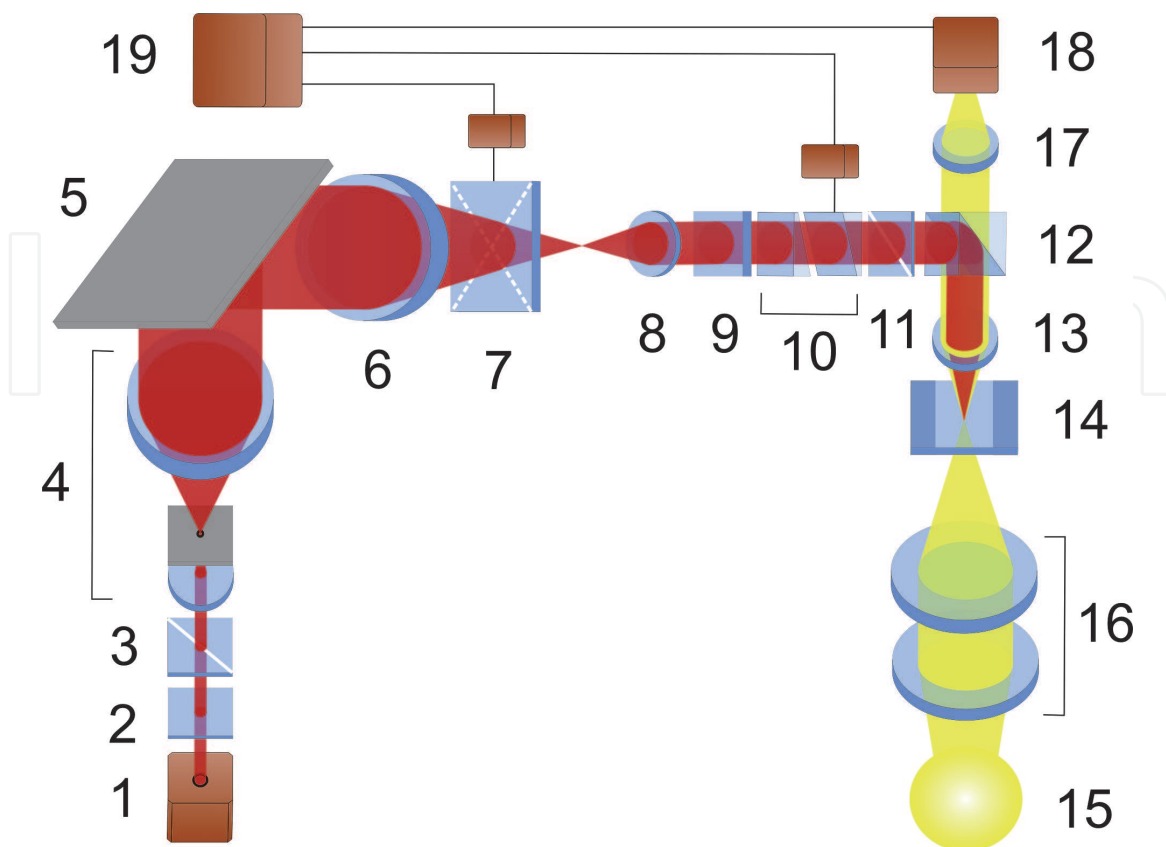


Figure 2.
Optical arrangement of tweezers based on a birefringent crystal.

2.3 Micro and nanoparticles as field probes

Our next achievements [11–14] demonstrate the results obtained by separating the contribution of the orbital and spin angular momentum to the total picture of trapped particles motion in the optical field.

To identify the internal spin energy flows [12], it was necessary to analyze the mechanical action of the spin momentum by testing, selecting size and property of the particles. The spin momentum manifests itself “in its pure form” with all the specific properties in the situation of a symmetric superposition of circularly polarized plane waves and thus the formation of a circularly polarized field having inhomogeneous energy (**Figure 3**) [11, 13]. The mechanical action of the incident field on test particles, when including the scattering components, was carried out through the calculation of the Cartesian components of the force (F_x , F_y , F_z) acting on particles that are placed in the optical field. The longitudinal component of the force (F_z) represents the traditional action of light pressure, which direct the particles forward; the transverse y-component (F_y) corresponds to the gradient force (F_y^{grad}) of an inhomogeneous optical field and traps particles or repels them from areas of high concentration of electromagnetic energy. The most interesting result is the analysis of the component F_{sp}^{\pm} of the optical power along the transverse direction F_x - the only component of the force that is associated with the spin flow. This conclusion is confirmed by the fact that, in accordance with the behavior of the spin flow, the value of the force F_x changes its sign with a change of the helicity σ of the incident beam. In the case of linearly polarized light, this component of the force completely disappears.

Despite the mechanical equivalence of spin and orbital energy flows, that is, their ability to cause translational or orbital motion of the particles under study, the quantitative features of spin-induced and orbital-induced motion, their dependence on the size and properties of the particles are significantly different. That is, the effect of spin and orbital flows can be experimentally distinguished by using test particles with specially selected size and properties. The following figure (**Figure 4**) [13] shows the dependence of the components' value of the optical forces on the particle size for different types of particles. The calculations were performed for two types of spherical particles suspended in water ($\epsilon = 1.77$, $\mu = 1$, $n = 1.33$): metal (gold hydrosol, relative refractive index $m = 0.32 + 2.65i$ [18]), dielectric (latex in water, $t = 1.12$); wave number $k = 1.33 \cdot 10^5 \text{ cm}^{-1}$ (He-Ne laser).

To eliminate the influence of the incident beam intensity and reduce the number of data presented, the obtained value of the force was normalized by dividing the calculated values by the total momentum of the incident flow over its cross section (P_0). A comparative picture of the mechanical action of the optical forces associated with the spin and orbital internal energy is presented in **Figure 4**. To compare the

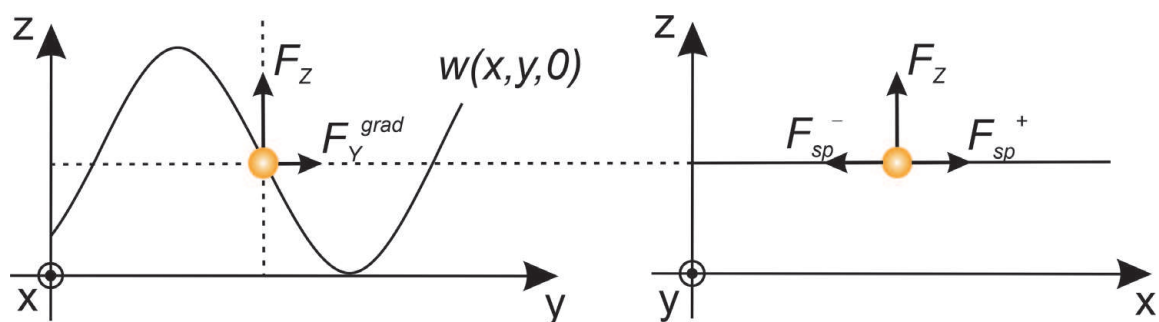
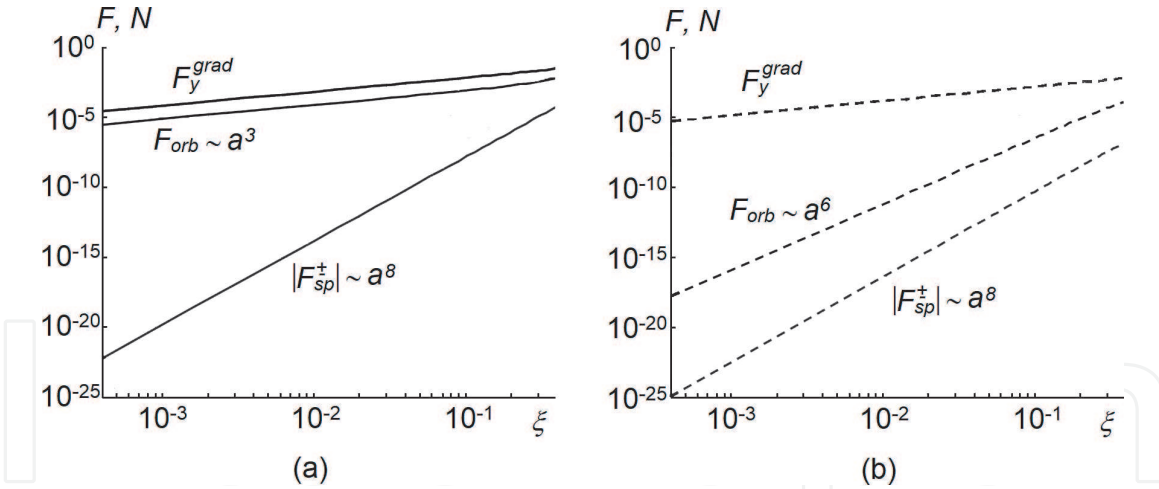


Figure 3.
 The components of optical force distribution.


Figure 4.

A comparative picture of the mechanical action of the optical forces associated with the spin and orbital internal energy for different types of particle: a) metal and b) dielectric.

optical force, the gradient force F_y^{grad} is shown. The measured gradient force range is 10^{-4} to 10^{-6} Newton, depends on the particle size and its type and determines the measurement accuracy as 10^{-7} Newton.

The curves are made for particles of small size. Solid lines describe metal particles, dotted lines describe dielectric particles. Here $\xi = ka$ is a dimensionless particle size parameter (a – is the particle radius).

As can be seen from the results of estimating the values of spin and orbital flows shown in the figure, the quantitative features of spin-induced and orbital-induced motions and, accordingly, the generated optical forces, their relationship with the size and properties of the particles are significantly different. Following the main aim of this paper, conducting optical power measurement according to the evaluation results (**Figure 4**), we can note the measured quantity of optical force up to 10^{-15} – 10^{-25} degree for the spin-induced component of the optical force in accordance with the particle size. We managed to carry out experimental confirmation of the existence of a force of this units of Newton in a specially organized experiment [11–13]. The use of dielectric test particles of the Rayleigh light scattering mechanism made it possible to evaluate experimentally the action of spin and orbital flows. Particles are sensitive to optical forces caused both by spin and orbital flows.

Thus, the change of the measured component of the optical force leads to the change of the measurement range of: the value of the optical force associated with the spin internal energy as 10^{-25} to 10^{-10} Newton, for different types and size of particle, with the error of 10% and the value of the optical force associated with the orbital internal energy as 10^{-16} to 10^{-6} Newton with the error of 7%.

The value of the force is estimated at the pico-, femto- Newton, and in accordance to our experiments (**Figure 5**) [11] the obtained results can be considered as a proof of the mechanical action of the spin moment (spin energy flow) of the light beam on test particles of the chosen shape and properties. The experimental observation of the polarization-dependent orbital motion of test particles in a transversely inhomogeneous beam with circular polarization, where the rotational action of the orbital momentum density is absent or insignificant, is here demonstrated. Moreover, this demonstration of motion required an ultra-precise experiment, when the peculiarities of measured quantity of optical force of the femto units of Newton is taken into consideration.

In order to observe the action of optical flows on nanoparticles, an optical scheme was chosen in which the lens aperture was selected in order to avoid

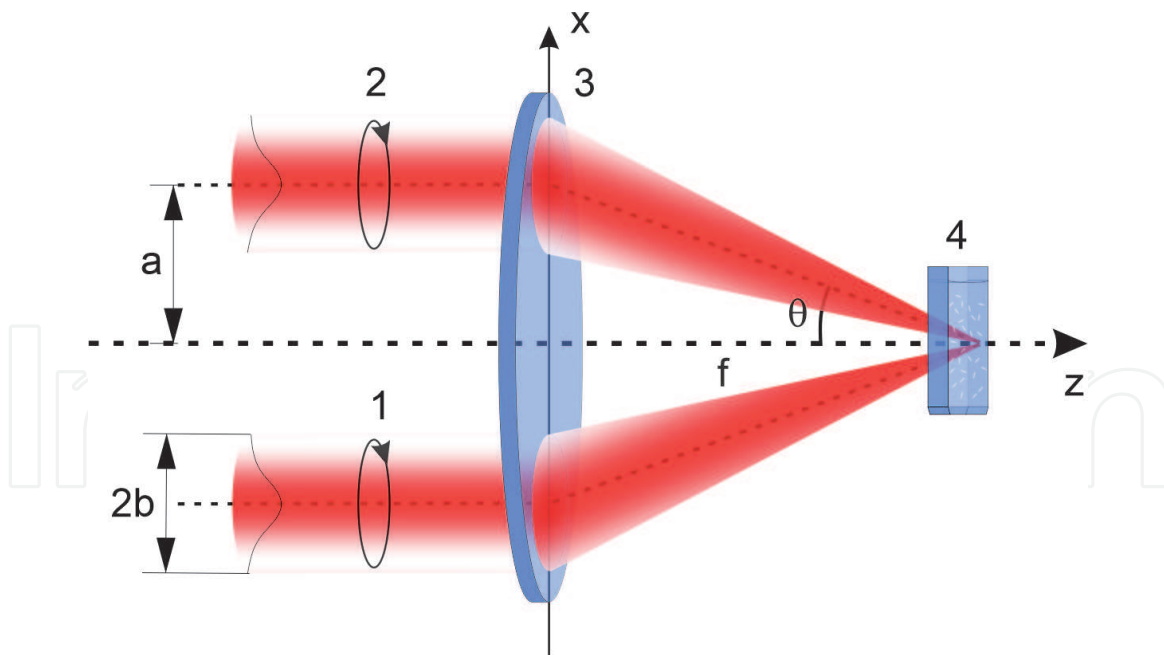


Figure 5.
Scheme of the experimental setup: (1), (2) - input beams; (3) objective lenses; (4) cuvette with test particles suspended in water.

transforming conversion of spin and orbital flows. Significant numerical apertures do not allow one to study the action of the spin momentum density, since strict focusing of a circularly polarized beam causes a partial transformation of the output spin flow into an orbital one. And even if some mechanical action of the flow is observed, then it is impossible to definitely conclude about the spin or orbital momentum action. To avoid ambiguity, focusing should not be high: the spin-orbital transformation can be neglected (i.e., it does not exceed 1%) when using lenses with a numerical aperture < 0.2 (angle $\theta \approx 11^\circ$).

Such focusing leads to a certain loss of energy concentration; however, a substantial decrease of the spin action in the focal region can be avoided if the decrease in intensity is compensated by an increase of the beam inhomogeneity. The above experimental design made it possible to reproduce and record the action of the optical force at the femto units of Newton, which is a unique confirmation of the present measurements' opportunity. The circulation of energy of a spin nature exists within each band, while the orbital momentum is completely radial and is associated with the beam divergence (**Figure 6**) [11]. This radial field momentum can be used to explain the mechanism of particle capture into the desired position outside the center, which allows one to observe the orbital motion associated with the density of the spin momentum.

In an inhomogeneous light field, any dielectric particle is exposed to the action of the gradient force that directs it to the maximum intensity, for example, to the axis of the beam, and vice versa. The radial density of the orbital momentum of the diverging beam creates a value of radial pressure that directs the particle away from the axis. As a result, both forces cancel each other out in certain areas of the interference pattern.

So, by changing the circulation of the electric field vector, the captured particle carries out orbital motion being it clockwise (**Figure 6A**) or counterclockwise (**Figure 6B**) rotational motion with respect to its own axis. Both the orbital and rotational motions stop when the polarization of the incident beam is linear. The possibility of particle transfer by the force induced by the influence of spin energy flows opens up new prospects for the creation of controlled optical micromachines,

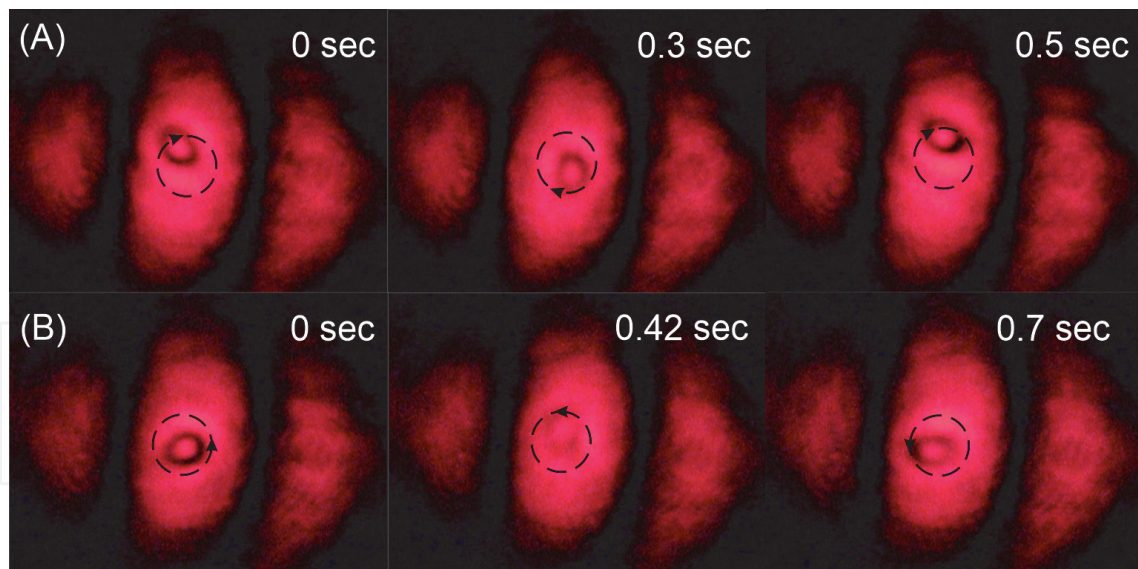


Figure 6.

The position of the captured particles within the center of the interference band at different moment of time with the change of the electric field vector circulation: A) clockwise, B) counterclockwise. The arrows indicate the direction of particle rotation.

micromanipulators in which the regulation and switching are performed through polarization control without changing the beam intensity or its spatial profile. Such methods can be useful in many systems requiring high switching speed.

It should be kept in mind that a nanoparticle is a multifunctional nanoscale tool, playing the role of a separate probe for diagnosing the field structure in the zone of a complex field microdistribution. These nanoparticles are the means of delivering microdoses of drugs into cells, and the unique means of studying complex macrostructure of the optical field in almost real time. Such a possibility can be realized in water or other transparent solutions, when the concentration of nanoparticles in various areas of the complex optical field, their spatial distribution will provide information on the spatial distribution of the amplitude, polarization, and, as a result, the phase of the field. There is an expected forecast for the study of speckle fields by nanoparticles, when they are transferred to the points of field singularity by internal energy flows, making it possible to restore information about changes of macro and micro objects over time.

2.4 Evanescent fields for micro-object manipulation

To talk about the influence of an optical field on nanostructures is necessary in order to distinguish the action of evanescent optical fields of a complex energy distribution, in particular to transfer of microdoses of drugs, providing precise accuracy of the transfer site and the transfer rate of hundreds of nanometers per second [18–20]. This situation becomes possible in the case of excitation of evanescent fields by linearly polarized beams with the azimuth of polarization of 45° . The evanescent field formed in such a way has a special distribution of spin and orbital momentum, it is elliptically polarized, in which the energy circulation is fixed in two planes - a plane parallel to the interface between the two dielectrics, where there is total internal reflection and in the plane perpendicular to it. A specific feature of the excitation of evanescent waves using a linearly polarized wave with azimuth of polarization of 45° is that the transverse spin component, which is responsible for the transverse component of the optical power appears.

In a paper [21], direct measurement of an optical momentum, which is called as extraordinary, and helicity dependent force directed perpendicularly to the

Poynting vector propagation, being proportional to the ellipticity of the local polarization of the probing beam has been reported. Such a complex structure of optical force takes place for evanescent waves and other structured fields being associated with the spin-momentum part of the Poynting vector. The extraordinary transverse momentum has been measured using a femto-newton resolution nano-cantilever immersed in an evanescent optical field above the total internal reflecting glass surface.

In our, later proposed experiments [22, 23], we use a free-standing plate for detection of the influence of an evanescent wave. We demonstrate an optically transparent birefringent microplate motion, influenced by the optical forces generated at the plate plane due to the complex optical force action: caused by the canonical momentum directed along the wavevector and the transversal spin momentum [24] directed perpendicularly to the canonical momentum. In this case it is possible to observe the motion of the plate in the direction, which does not coincide with any of these directions. The surfaces of a birefringent plate are characterized by the negligible roughness. We deposited gold nanoparticles at plate's upper surface to transfer the transverse momentum to the plate.

Elliptically polarized wave formed at a sup-surface layer enables us to estimate the longitudinal and transversal components of the force. Therefore, the vertical spin of an evanescent wave is the source of the last of them.

We simulate the spin and orbital momenta of an evanescent wave when a linearly polarized incidence wave (at second surface - boundary plate-air) with the azimuth of polarization 45° reaches the interface plate-air here undergoing total internal reflection (TIR). In this case, an evanescent wave that propagates in the z-direction, being damped in the x-direction, can be represented by [21, 24].

$$\vec{E}_{ev} = E \exp(-i\omega t) \left(\vec{x} \frac{1}{\sqrt{1+|m|^2}} + \vec{y} \frac{m}{\sqrt{1+|m|^2}} \cdot \frac{k}{k_z} + \vec{z} (-i) \frac{1}{\sqrt{1+|m|^2}} \cdot \frac{k}{k_z} \right) \cdot \exp(ik_z z - kx), \quad (1)$$

where $k_z = k \frac{n_o}{n} \sin \gamma$, $\kappa = k \sqrt{\left(\frac{n_o}{n}\right)^2 \sin^2(\gamma) - 1}$ is the exponential decay rate.

Here, $v m = \frac{T_{\perp}}{T_{\parallel}} m_1$ is a state of polarization of an evanescent wave [24], m_1 is the state of polarization of the beam impinging at the interface plate-air being equal to unity for linear polarization with the azimuth of polarization 45° . γ is the angle of incidence at the surface, where TIR takes place.

$E = \frac{k_z}{k} \sqrt{\frac{\mu_1}{\mu}} T E_0$ is The electrical strength of the field of an evanescent wave,

where $T = \frac{\sqrt{|T_{\parallel}|^2 + |m_1|^2 |T_{\perp}|^2}}{\sqrt{1+|m_1|^2}} \exp[i \arg T_{\parallel}]$ is the transmission coefficient [22], and T_{\parallel}, T_{\perp} are the Fresnel transmission coefficients.

In this case the spin momentum density has both longitudinal and transversal components [24].

Thus, the resulting momentum density in the z-direction possess both orbital and spin momentum density and is given by

$$p_z = p_{oz} + p_{sz} = \frac{A^2}{8\pi\omega} \left[\left(k_z + \frac{m^2 k^2}{k_z} + \frac{\kappa^2}{k_z} \right) - 2 \frac{\kappa^2}{k_z} \right] \exp(-2\kappa x). \quad (2)$$

The transversal momentum caused by the vertical spin is represented as.

$$p_y = p_{sy} = \frac{A^2}{4\pi\omega} \frac{k\kappa}{k_z} \text{Im} m \cdot \exp(-2\kappa x), \text{ where } A = E \frac{1}{\sqrt{1+|m|^2}}.$$

We change the angle of incidence of a beam at the boundary plate-air. It leads to changing of the ellipticity of the evanescent wave above the plate surface. That is why one can suppose that the magnitude of the transversal spin momentum could be characterized by the different dependence towards to the resulting momentum in the longitudinal direction with the main contribution by the canonical momentum. We suppose that momentum is transmitted to the spherical surface S of the gold particles localized at the plate surface. Particle's light-scattering is taken into account within the Mie approximation [24], giving $\vec{F} = \int_S \Delta\vec{p} dS$, where $\Delta\vec{p}$ is the change of momentum density. Simulation of the force affecting a plate and causing its motion presumes integration over the illuminated area with beam aperture of 6° . The results of optical forces simulation in the y - and z -directions for a linearly polarized incident beam with the azimuth of polarization of 45° versus the incidence angle γ are shown in **Figure 7**.

As can be seen from the presented results, the transversal component of the optical force acting from the evanescent field on gold nanoparticles is experimentally fixed in our studies. Experimental study has shown that the motion of the birefringent plate depends on the angle of incidence of the beam which generates the evanescent wave. The incidence angle influence both velocity and spinning of the plate, as well as the angle of deviation of the ahead motion from the z -axis.

Thus, our experiments [22, 23] demonstrate simultaneous plate rotation and forward plate motion. The rotation of the plate stops in the situation when the main optical axis of the plate coincides with the azimuth of polarization of the incident beam. The compensation of birefringence torques leads to vanishing of plate rotation. This is observed precisely for linearly polarized wave impinging onto the second surface of a plate at an angle $\pm 45^\circ$. It is achieved for an angle of incidence of the probing beam about 58° which gives the azimuth of polarization of this beam at the first plate interface (boundary air-plate) equal to 62° . Therefore, rectilinear motion of the plate without its rotation is possible due to the action of the

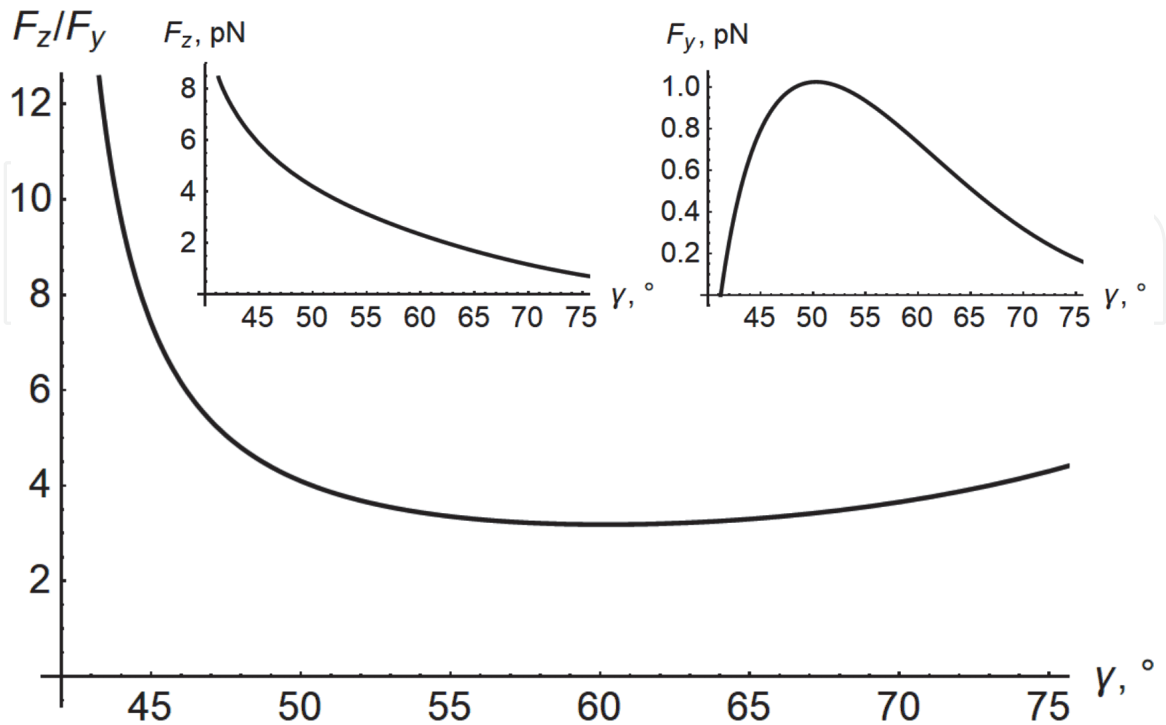


Figure 7. The ratio of optical force in the longitudinal and transversal directions (F_z/F_y) with insets, described the resulting force in the z -direction (F_z) and the transverse diagonal polarization-dependent force induced by the vertical spin momentum in the y -direction (F_y), as a function of the incidence angle γ .

transversal component of the optical force generated above the plate. The angle between the motion direction and z-axis is 15°.

The use of these effects for evanescent waves [25, 26], in particular, is relevant for the development of nanotechnology, including molecular, especially for biomedicine, nano-therapy, transportation of medical products, bio-marking, cancer diagnosis, and bio-probing. All this provides a new tool to investigate the cell properties, i.e. mechanical or optical parameters and characteristics [26].

This brings about non-invasive methods for evaluating and analyzing pathological changes in tissues with the search for new opportunities for treating diseases and possible pathologies by non-traumatic, easily accessible methods.

2.5 Measurement of optical parameters for low-absorbing microparticles

The next step of our paper is to demonstrate one of the solutions for measurement and determining the absorption coefficient of low-absorbing microparticles by estimating the rotation speed of such objects in the field of a circularly polarized beam [27]. The uniqueness of the proposed experimental approach is that the measurement error in determining the optical parameter is of the order of femto units. It is a confirmation of the breakthrough in optical metrology and relies on the fact that modern experimental equipment and corresponding experimental approaches and measurements have gone out of the microrange to a new, more delicate level.

In particular, we present results obtained by studying the microscopic properties of liquids and various biological samples by complex optical fields [28, 29]. The optical field, acting on particles, transfers part of the momentum to them, thereby causing the spatial motion of the particles. The characteristics of this motion substantially depend on the optical constants of the studied micro- and nanoparticles.

Even the properties of complex solid samples containing, as impurities, various kinds of inclusions in the form of a fine-grained structure are determined by the optical properties of these micro and nanoparticles, thereby opening for applications. A change of the radiation propagation conditions substantially depends on the attenuation of the radiation, here determined by the absorption and scattering of radiation on these structures.

Traditionally, solutions to such problems are sought through using of Mie scattering theory, which allows one to determine mechanical ponderomotive factors (force and torque) which an optical field exerts on a particle. More importantly, the ponderomotive factors can be directly associated with the optical parameters of the particle, and this can be employed for their measurement.

In [27], the criterion of optical fields action on micro- and nano-particles is the rotational motion of the particle under the influence of a torque, which is inherent in an optical field of circular polarization with a spin angular momentum. The spinning motion of the particle is due to the field spin angular momentum absorbed by the particle, and its angular velocity Ω is related to the radiation torque by the equation $\Omega = \frac{T}{8\pi\eta r^3}$, where $\eta = 8.9 \cdot 10^{-3} \text{ dyn} \cdot \text{s} \cdot \text{cm}^{-2}$ (at 25°C) is the dynamical viscosity of the medium. T is an absolute torque, which is calculated through Mie theory $T = 4\pi I \frac{n}{c} \sigma \left(\text{Im}(\alpha_e) - \frac{2k^3}{3\epsilon} |\alpha_e|^2 \right)$, here α_e – is the polarizability, appears due to the particle absorption. I is the energy flow density in the wave, c is the light velocity in vacuum, ω is the wave frequency, $k = (\omega/c)n$ is its wavenumber, and σ is the wave spin number equal to ± 1 for right (left) circular polarization, respectively, and 0 for any linear or no polarization. Here the particle is assumed to be immersed in a homogeneous isotropic dielectric medium with real permittivity ϵ and real permeability μ so that the refraction index equals to $n = \sqrt{\epsilon\mu}$.

The absorption index κ of the particle suspended in water and trapped in the center of a focused Gaussian beam waist with radius $w_0 = 2 \mu\text{m}$ can be directly derived from the observed spinning velocity Ω exhibited by the particle in the beam with power $P = 100 \text{ mW}$, $\kappa = q \frac{\Omega}{P}$, where q is the transition coefficient. At the same time, the particle must be with low absorption, so that there is no local heating of the medium surrounding the particle. Effective particle capture requires that the particle size be several times smaller than the size of the focusing spot, but in such a way as to prevent diffraction by the captured object. We have used weakly absorbing ($\kappa \leq 10^{-3}$) dielectric particles with diameter 0.5 to $2 \mu\text{m}$. A schematic of the experimental equipment [27] is presented in the following **Figure 8**. This setup consists of a laser – 1, a beam expander with spatial filter – 2, a mirror – 3, a quarter-wave plate – 4, objective lenses – 5, 7 and 8, cell with probing particles suspended in water – 6, CCD-camera – 9, a personal computer – 10, a control unit – 11.

As a result of the optical field action, the particle acquires a rotational motion, and the angular velocity of the particle corresponds to the part of the torque that is absorbed. As absorption increases, acceleration of rotational motion is observed. The measured value of the spinning velocity obtained in the experiment, e.g. for a gamboge particle is of about $\Omega_e = 25.8 \text{ s}^{-1}$, a measurement range of the spinning velocity is $25.8 \text{ s}^{-1} \pm 0.3 \text{ s}^{-1}$, the standard measurement uncertainty is 0.13 s^{-1} with the normal probability distribution. The average measured value of the spinning velocity differs from the theoretically obtained spinning velocity and determines the error of about 20%.

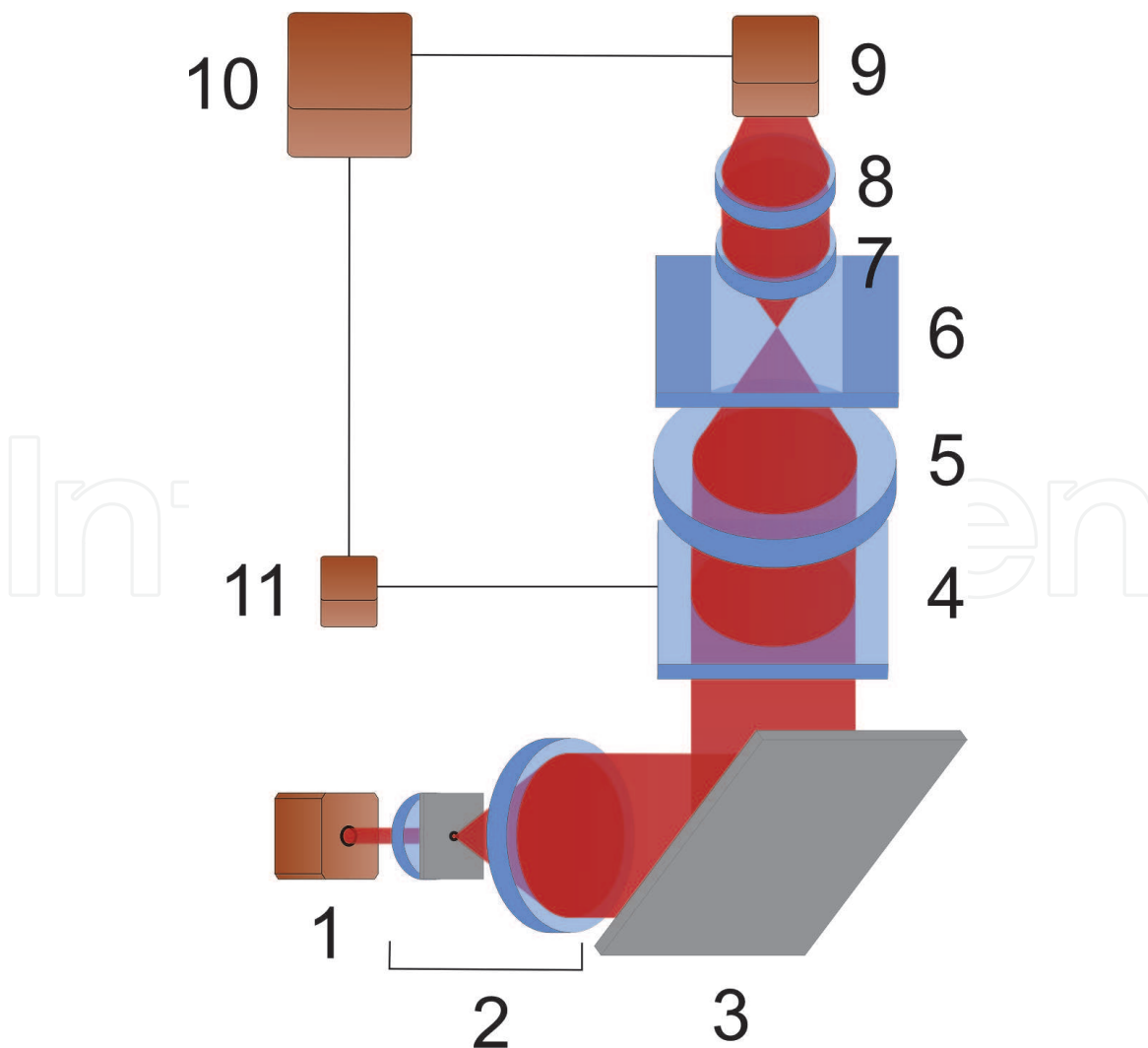


Figure 8.
Schematic of the experimental setup.

Such an error can be explained by the longitudinal displacements of the particle with respect to the beam waist, heating of the cell with particles, changes in the properties of water inside the cell, and other reasons. The introduction of the normalization coefficient, obtained by comparing the theoretical and experimental results, made it possible to determine the value of the particle absorption coefficient, here for this type of particle, it was $12.4 \cdot 10^{-4}$.

Of course, the question arises about the measurement error of the proposed method for measurement the absorption index. The flexibility of this method is determined by the refractive properties of the particle, the density of the medium where the particles are dispersed, the characteristics of the irradiating beam, and the cross-section of the focused beam. Restrictions for the determination of the particle rotation speed of about 0.1 s^{-1} are formed. Then, with the introduction of transition coefficient (q), the error in estimating the absorption coefficient δ can be obtained in the range $10^{-8} \leq \delta \leq 4 \cdot 10^{-7}$. Obtaining reliable results of measurement the absorption coefficient of particles is possible for absorption less than 10^{-2} .

Thus, the possibility of directly assessing the value of the index of light absorption by microparticles became possible thanks to the proposed approach, which uses the principles of capture and rotation of microparticles by internal energy flows. The current state of the development of technology for the manipulation of microobjects of various nature and properties makes the proposed method of measurement of optical properties encouraging and promising for many practical applications. The obtained results are the first step in developing of this kind of measurements. The high sensitivity of the absorption index measurement, the high accuracy of the estimation of the measured parameter, upon reaching the appropriate level of control for the measurement conditions, makes it possible to use this method to study weakly absorbing particles.

The above mentioned results on the involvement of the technique of micro and nanoparticles in the study of complex optical fields, the transition to control of the particle movement within a few angstroms with the acting force on the captured object at the femto Newton unit are opened the new possibilities of modern metrology. Such approaches are already used today to manipulate organelles in cells, to study viscoelastic properties, to build molecular motors and find their implementation among many other interesting applications.

2.6 Surface nanostructure and optical measurements

The next step in presenting the results of research and development on the latest methods of optical metrology is diagnostic methods for processing extremely smooth surfaces with ultra-high precision accuracy [28, 29].

Two techniques for measurement of roughness, based on measurement of a phase variance of the boundary object field and on a transverse coherence function of a field, as well as the devices implementing these techniques were proposed in our papers [28, 29]. The following principles are lying in the base of the proposed techniques:

- heights of surface microirregularities are less than wavelength of the probing radiation, ($R_q < 0.1 \text{ mm}$), and the transversal scale of surface irregularities is larger than a wavelength, so that the specular component of the reflected radiation is present;
- phase variance is measured at the boundary field (the sample surface is imaged at the plane of analysis); the transversal coherence function of a field can be measured at arbitrary zone;

- statistical parameters of a field are measured with interferometric means, within the zero (infinitely extended) interference fringe.
- The first technique (**Figure 9**) is used for measurement of surface roughness based on measurement of a phase variance of the boundary object field [30].

Here the experimental arrangement (**Figure 9**) consists from He-Ne - laser, T - telescope, BS1, BS2- beam-splitters, O1,O2 - objective lenses, S - sample, M - mirror, PM – piezo-ceramic modulator, PD - 2x2 position-sensitive photodetector array, VC- visualization channel, EM - electric motors, AU - automatic zero fringe adjustment unit, COM - comparator, CU - analogue R_q calculation unit, DI - digital indicator.

Using an interrelation among the height parameters of surface roughness and the phase parameters of the boundary object field, one obtains the following

equation for an root mean square deviation (RMS) roughness: $RMS = \frac{\lambda}{4\pi} \sqrt{\frac{\langle I(x,y) \rangle}{I_0}}$.

Technical parameters of the device are the measured RMS range – 0.002 to 0.08 μm , the measurement accuracy - 0.001 μm , the measurement scheme – micro-interferometer, indication rate - one measurement per five second, indicated units – micrometers. Here $I(x,y), I_0$ are the resulting field and the object beam intensity correspondingly.

This device could be used for measurement of the plane and spherical surfaces with the radius of curvature larger than 0.2 m in polishing machine tool for surface quality control during making of details. This device can be made as a stationary instrument.

The second one is a technique for measurement of surface roughness based on measurement of a field's transverse coherence function (**Figure 10**) [29].

For measurement of the degree of arbitrary surface roughness in the second technique we have proposed an experimental arrangement (**Figure 10**) with

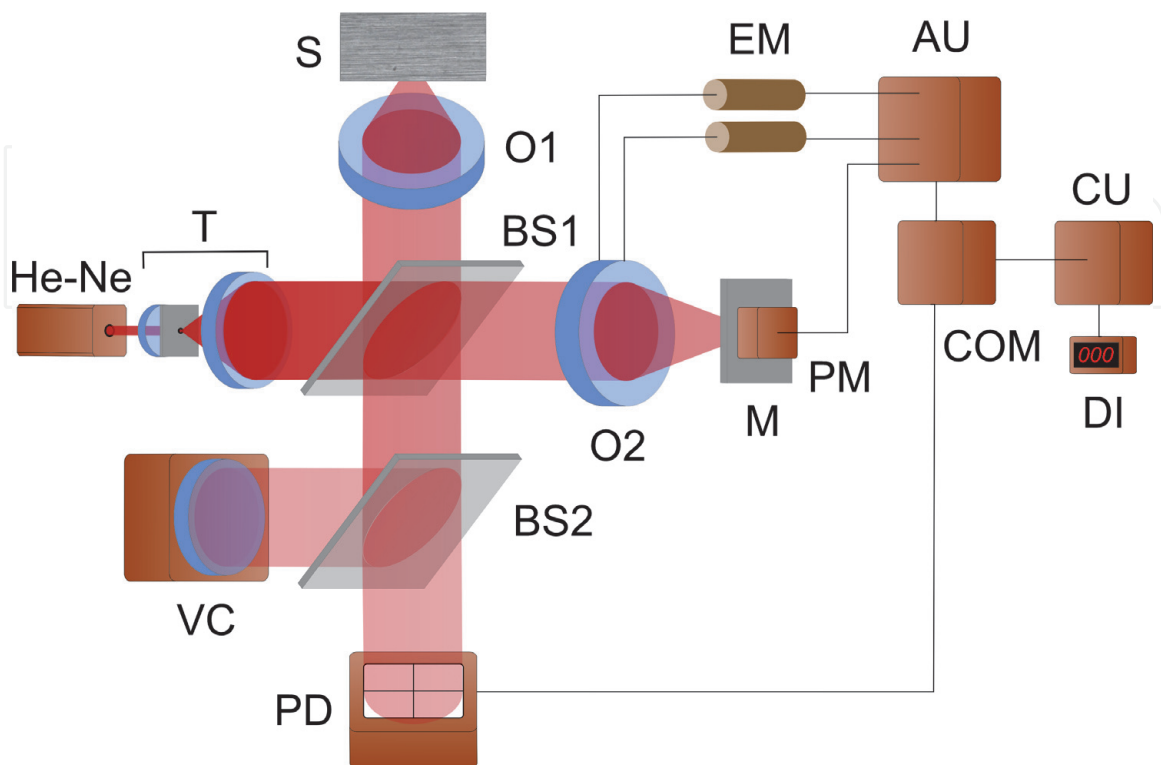


Figure 9.
Experimental arrangement for measurement of the degree of low-reflectance surface roughness.

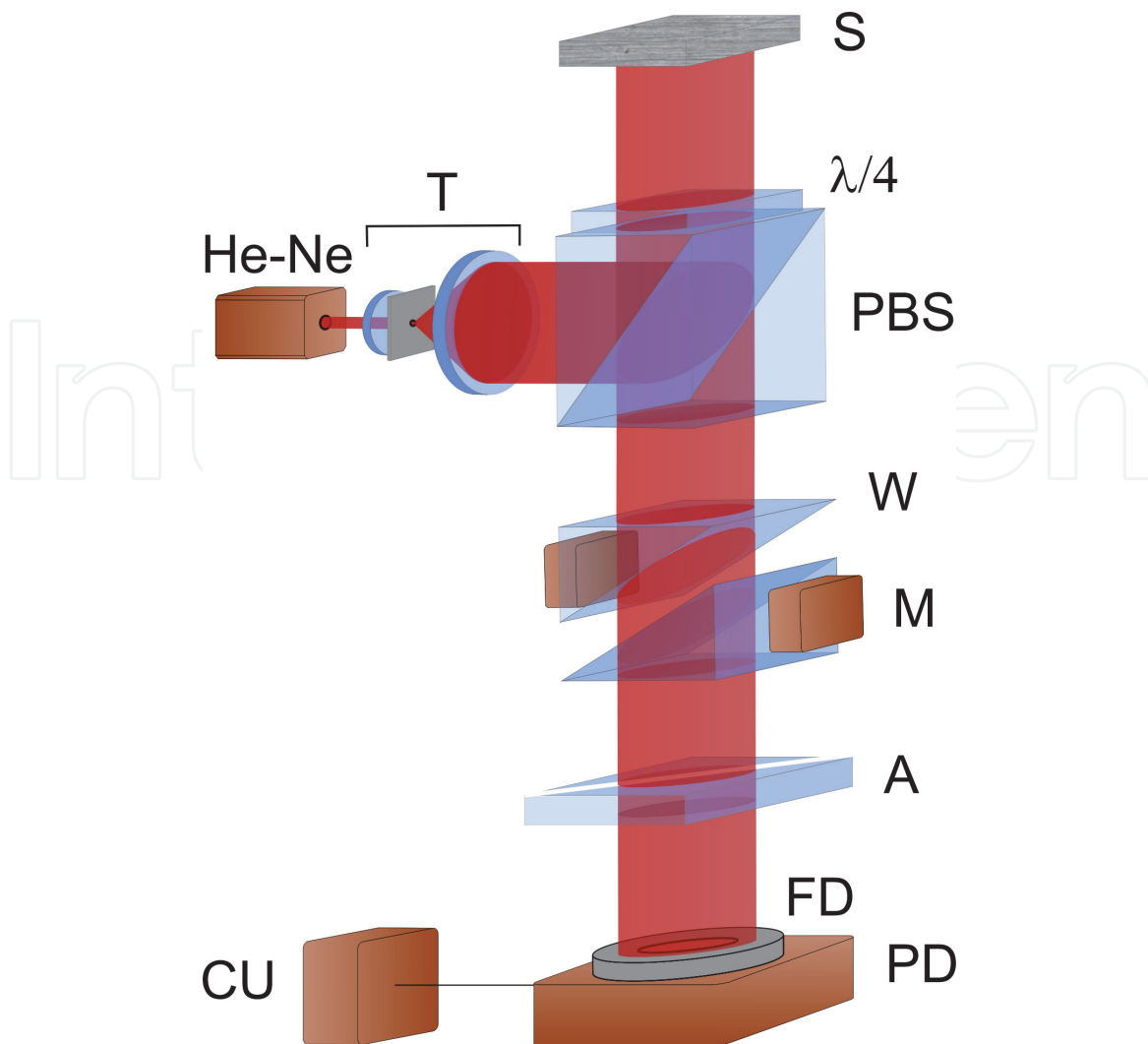


Figure 10.
 Experimental arrangement for measurement of the degree of arbitrary surface roughness.

He-Ne - laser, T - telescope, PBS- polarizing beamsplitter, S - sample, W- calcite wedges; M - electromechanical modulator, A - analyzer; FD - field-of-view diaphragm; PD - photodetector, CU - analogue R_q calculation unit.

Another method for measurement of the phase variance utilizes the relationship between the transverse coherence function $\Gamma_{\perp}(\rho)$ of the scattered field, on the one hand, and the statistical parameters of the object, on the other hand. The RMS height deviation can be found from the relation $RMS = \frac{\lambda}{4\pi} \sqrt{-\ln \frac{I_{max} - I_{min}}{I_{max} + I_{min}}}$, I_{max} , I_{min} are the maximum and minimum resulting intensity, respectively. The information contained in the resulting interference pattern is extracted by transforming the optical signal into electric ones with subsequent processing in the analogue electronic unit CU.

Two versions of the device for a surface roughness control based on measurement of the field's transverse coherence function were displayed:

- A stationary device that can be mounted on the processing tool. Device intended for measurement of the RMS height deviations of slightly rough surfaces over the range from 0.002 μm to 0.06 μm . Technical parameters are measured RMS range – 0.003 to 0.10 μm , measurement accuracy - 0.002 μm . Update rate - one measurement per second. Fields of application are the following: the photochemical industry to analyze the quality of calendar shafts; arbitrarily shaped surfaces with the radius of curvature larger than 0.3 m;

polishing machine tool; space industry to monitor the quality of mirrors fabricated by diamond micro-sharpening. This device was used for surface quality on-line control.

- Portable device for control of large-area or small-area surfaces. Portable device intended for measurement of the RMS height deviations of slightly rough surfaces. Main technical parameters of the device are the measured RMS range – 0.005 to 0.10 μm , the measurement accuracy - 0.002 μm , the update rate - one measurement per second. This device provides the following field of application: device can be made either as a measuring head, or as a stationary instrument, depending on the size and the position of the object to be controlled; polishing machine tool, this device was used for the surface quality control during making of the detail;

Sensitivity of the RMS height parameter of all these devices down to 10 Å was achieved. Roughness control of slightly rough (polished) surfaces with RMS deviation of a profile from a mean surface line ranging from 0.002 μm to 0.10 μm . The technique is applicable to metallic, insulator, semiconductor, and optical surfaces.

2.7 Optical refractive index measurement

At last it would like to bring one more aspect of fine measurement related to the determination of such an optical parameter of the studied object as the refractive index of light-scattering liquid media. Here, a specific issue is polarization interferometry to find the refractive index of solutions, suspensions and gaseous media [31]. According to the proposed approach [31], a two-beam interferometer is used to determine the refractive index, in which a circularly polarized beam is formed in each channel. The measurement method consists in splitting the optical radiation into two components and forming mutually orthogonal circular polarizations of the field components. As a result of superposition of such beams, a uniform intensity distribution is seen in the interference plane. In this case, the formed field has some deterministic polarization. The resulting field is linearly polarized and is characterized by the azimuth of polarization α_0 . When the studied solution is located in the object channel giving rise to polarization change of the transmitted radiation.

As a result, a rotation of the azimuth of linear polarization is observed in the interference plane, which takes on the value α . That is, the difference in polarization azimuth $\alpha - \alpha_0$, which is related to the reduced path difference of the beams in the arms of the interferometer, and is given by $n = n_0 + \Delta n_0 = n_0 + \frac{(\alpha - \alpha_0)\lambda}{2\pi l_0}$, where n_0 is the refractive index of the main medium (solvent), l_0 is the cell thickness.

The azimuth of polarization of the resulting distribution is sensitive to variations in the path difference in the arms of the interferometer. Even with a change in the path difference between the orthogonal components by an amount less than λ , the polarization azimuth will change significantly. If the path difference between the orthogonal components is λ , then the polarization azimuth will change by 2π . The polarization azimuth can be measured with a measurement error of some seconds. As a result, the accuracy of path difference measurement (Δl) is $10^{-5}\lambda$, and the measurement accuracy of the value of the refractive index is $10^{-6} \frac{\lambda}{l_0}$.

2.8 Biomedical application of 3D laser polarization metrology

Now we will try to present some last results on the development and experimental testing of a new 3D Stokes-polarimetry method for mapping the object fields

of biological optically anisotropic layers [8–10]. Particular, we propose digital holographic layer-by-layer reconstruction of polarization ellipticity distributions to express diagnostic and differentiate of polycrystalline blood films samples of patients with prostate tumors. The structural-logical diagram and design of 3D layer-by-layer Stokes-polarimetry method are described by **Table 1**.

The proposed optical scheme is shown in **Figure 11**.

Collimator 2 forms a parallel ($\varnothing = 2 \times 10^3 \mu\text{m}$) beam of He-Ne ($\lambda = 0.6328 \mu\text{m}$) laser 1, which is divided by 50% beam splitter 3 into “irradiating” (*Ir*) and “reference” (*Re*) ones. The “irradiating” beam is directed through the polarizing filter 6–8 by the rotating mirror 4 on the sample of the biological layer 9. The polarization-inhomogeneous image of the object 9 is projected by the lens 10 into the plane of the digital camera 15. The “reference” beam is forwarded by the mirror

1	Optical probing source	Gas helium-neon laser; Wavelength $0.6328 \mu\text{m}$
2	Block for forming the spatial structure of the optical probe	Optical collimator for forming a parallel laser beam with a cross section of 5 mm
3	Block for the formation of the polarization structure of the optical probe	System of formation of linear (0° , 90° , 45°) and right-circular polarization (linear polarizer.
4	Object block	Microscopic coordinate node
5	Formation block of microscopic image	Polarizing micro lens
6	Multichannel polarization filtering block	Transmission system of linearly (0° , 90° , 45° , 135°), right- and left-circularly polarized components
7	Reference wave formation block	Polarizing beam splitter
8	Block for the formation of the polarization structure of the reference coherent wave	Linear (0° , 90° , 45°) and right-circular polarization system
9	Polarization filtering block	Linear polarizer
10	Discritization block	Digital CCD camera
11	Block for computer processing of polarization interferometry data	Calculation algorithms: <ul style="list-style-type: none"> • distributions of the magnitude of the ellipticity • statistical moments of the 1st - 4th orders.

Table 1.
 Structural-logical diagram of the method of 3D layer-by-layer stokes-polarimetry.

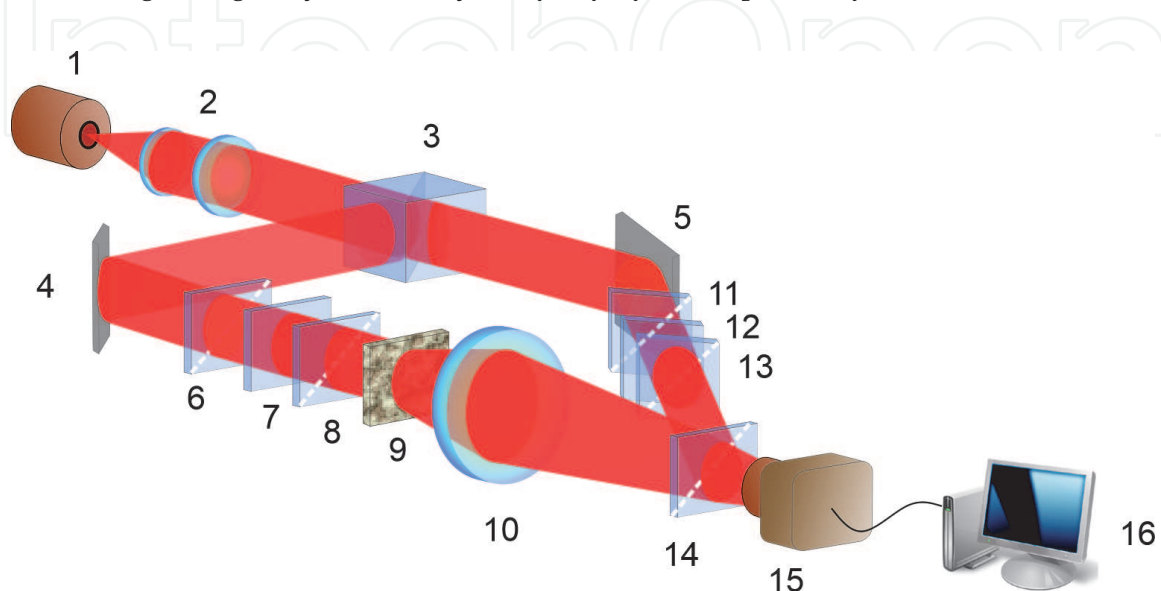


Figure 11.
 Optical scheme of 3D Stokes-polarimetry for polycrystalline blood films microscopic images.

5 through polarizing filter 11–13 into the object image plane 9. The resulting interference pattern is recorded by a digital camera 15 through the polarizer 14.

As a result, the topographic maps and histograms of statistical parameters and polarization ellipticity of layer-by-layer digital microscopic images of polycrystalline blood films of patients were measured and compared. It made possible to carry out a differential diagnostic of benign and malignant prostate tumors with different degrees of differentiation.

3. Conclusions

The results presented in this chapter provide an overview of the new approaches of measurements and results obtained by the authors of this chapter over the past decades, in the direction of ultra-sensitive precision measurements. In this chapter we have tried to present the metrological aspects of new optical measurements, that had made it possible to expand the range of measurement of such optical quantities as optical force and optical parameters of solid, liquid and gas up to femto and pico units. This improves the accuracy of optical measurements for the corresponding quantities by 3 orders of magnitude.

The sensitivity of the methods achieved by interference, polarization-interference when assessing the roughness of smooth surfaces, when measurement variations in the refractive index of aqueous solutions ranges from tens of angstroms to tens of nanometers.

The femto unit of optical forces, which occurs in complex optical fields with a rich morphology of the distribution of internal optical energy flows, interacts with micro- and nano-objects of various shapes and properties, but also control their spatial motion in optical traps, the nature of which can differ significantly in accordance with the trap formation mechanism. The optical forces of this physical nature and the values are used to determine the optical parameters of trapped particles, where the error of the determination is controlled at the nanoscale level.

The nature of the trap is different, but the original and new of our approaches are the use of biaxial crystals, which allowed us to form a complex distribution of internal energy flows and at the same time realize the conversion from phase-amplitude to polarization structures intended for nano-objects capture.

New polarimetric solutions for 3D Stokes mapping of microscopic images of polycrystalline blood films with digital holographic reproduction of layer-by-layer polarization maps of ellipticity with the success is shortly demonstrated in the given chapter.

It is clear that this review cannot be a complete analysis of new modern ultrathin methods of optical metrology. It is also worth recalling the ideas and principles of STED microscopy [32, 33], the physical principles of the operation of optical vortex coronagraphs [34], and much more. As an exclusive it could be noted the fundamentally achievable opportunity to operate and manipulate with atoms [2] - this is the ultimate fantasy for the optical range.

IntechOpen

Author details

Oleg Angelsky^{1,2}, Peter Maksymyak², Claudia Zenkova^{1,2}, Olexander Ushenko²
and Jun Zheng^{1*}

1 Research Institute of Zhejiang University, Taizhou, China

2 Chernivtsi National University, Chernivtsi, Ukraine

*Address all correspondence to: dbzj@netease.com

IntechOpen

© 2021 The Author(s). Licensee IntechOpen. This chapter is distributed under the terms of the Creative Commons Attribution License (<http://creativecommons.org/licenses/by/3.0>), which permits unrestricted use, distribution, and reproduction in any medium, provided the original work is properly cited. 

References

- [1] Hell S, Nanoscopy with focused light (Nobel Lecture), *Angew. Chem. Int. Ed. Review.* 2015; 54:8054–8066.
- [2] Rubinsztein-Dunlop H. et al., Roadmap on structured light. *J. Opt.* 2017; 19:013001.
- [3] Rotenberg N, Kuipers L, Mapping nanoscale light fields. *Nature Photon.* 2014; 8: 919.
- [4] Bauer T, et al., Observation of optical polarization Möbius strips. *Science.* 2015; 347: 964.
- [5] Geng J, Structured-light 3D surface imaging: a tutorial. *Adv. Opt. Photon.* 2011; 3: 128–133.
- [6] Ghosh N, Tissue polarimetry: concepts, challenges, applications, and outlook. *J. Biomed. Opt.* 2011; 16: 110801.
- [7] Vitkin A, Ghosh N, & de Martino A, Tissue Polarimetry. In: *Photonics: Scientific Foundations, Technology and Applications.* Andrews DL, editors. John Wiley & Sons, Ltd.; 2015, p. 239–321.
- [8] Angelsky OV, Ushenko A, Ushenko YA, Pishak VP & Peresunko AP. Statistical, Correlation, and Topological Approaches in Diagnostics of the Structure and Physiological State of Birefringent Biological Tissues. In *Handbook of Photonics for Biomedical Science.* Tuchin V V. editor. CRC PRESS; 2010, p. 283–322. doi:10.1201/9781439806296-c10
- [9] Ushenko VA, Hogan BT, Dubolazov A, Grechina AV, Boronikhina TV, Gorsky M, Ushenko AG, Ushenko YO, Bykov A, Meglinski I, Embossed topographic depolarisation maps of biological tissues with different morphological structures, *Scientific Reports* 2021; 11(1): 3871.
- [10] Peyvasteh M, Tryfonyuk L, Ushenko V, Syvokorovskay A-V, Dubolazov A, Vanchulyak O, Ushenko A, Ushenko Y, Gorsky M, Sidor M, Tomka Y, Soltys I, Bykov A, Meglinski I, 3D Mueller-matrix-based azimuthal invariant tomography of polycrystalline structure within benign and malignant soft-tissue tumors. *Laser Physics Letters* 2020; 17 (11): 115606.
- [11] Angelsky OV, Bekshaev AYa, Maksimyak PP, Maksimyak AP, Hanson SG, and Zenkova CYu, Orbital rotation without orbital angular momentum: mechanical action of the spin part of the internal energy flow in light beams. *Opt. Express* 2012; 20(4): 3563–3571.
- [12] Angelsky OV, Bekshaev AYa, Maksimyak PP, Maksimyak A., Mokhun II, Hanson SG, Zenkova CYu, and Tyurin AV, Circular motion of particles suspended in a Gaussian beam with circular polarization validates the spin part of the internal energy flow. *Opt. Express* 2012; 20(10): 11351–11356.
- [13] Bekshaev AYa, Angelsky OV, Hanson SG, and Zenkova CYu, Scattering of inhomogeneous circularly polarized optical field and mechanical manifestation of the internal energy flows. *Phys. Rev. A* 2012; 86(2): 023847.
- [14] Zenkova C, Soltys I, Angelsky P, The use of motion peculiarities of particles of the Rayleigh light scattering mechanism for defining the coherence properties of optical fields. *Optica Applicata* 2013; 43(2): 297–312.
- [15] Angelsky OV, Bekshaev AYa, Maksimyak PP, Polyanskii PV, Internal Energy Flows and Optical Trapping. *Optics & Photonics News (OPN)* 2014; 25.
- [16] Dienerowitz M, Mazilu M, Dholakia K, Optical manipulation of

- nanoparticles: a review. *J. Nanophoton* 2008; 2: 021875.
- [17] Bekshaev AYa, Subwavelength particles in an inhomogeneous light field: Optical forces associated with the spin and orbital energy flows. *J. Opt.* 2013; 15: 044004.
- [18] Angelsky OV, Maksymyak PP, Zenkova CYu, Maksymyak AP, Hanson SG, Ivanskyi DI, Peculiarities of control of erythrocytes moving in an evanescent field. *J. of Biomedical Optics* 2019; 24 (5): 055002.
- [19] Angelsky OV, Zenkova CYu, Ivanskyi DI, Mechanical action of the transverse spin momentum of an evanescent wave on gold nanoparticles in biological objects media. *Journal of Optoelectronics and Advanced Materials* 2018; 20(5–6): 217–226.
- [20] Angelsky OV, Zenkova CY, Maksymyak PP, Maksymyak AP, Ivanskyi DI, Tkachuk VM, Peculiarities of Energy Circulation in Evanescent Field. Application for Red Blood Cells. *Optical Memory and Neural Networks (Information Optics)* 2019; 28(1): 11–20.
- [21] Antognozzi M, Bermingham CR, Hoerber H, Dennis MR, Bekshaev AYa, Harniman RL, Simpson S, Senior J, Bliokh KY, Nori F, Direct measurements of the extraordinary optical momentum and transverse spin-dependent force using a nano-cantilever. *Nature Physics* 2016; 12: 731–735.
- [22] Angelsky OV, Hanson SG, Maksymyak PP, Maksymyak AP, Zenkova CYu, Polyanskii PV, and Ivanskyi DI, Influence of evanescent wave on birefringent microplates. *Optics Express* 2017; 25(3): 2299.
- [23] Zenkova CYu, Ivanskyi DI, Kiyashchuk TV, Optical torques and forces in birefringent microplate. *Optica Applicata* 2017; 47(3): 483–493.
- [24] Bliokh KY, Bekshaev AY, Nori F, Extraordinary momentum and spin in evanescent waves, *Nature Communications* 2014; 5.
- [25] Yoon Y-Z, and Cicuta P, Optical trapping of colloidal particles and cells by focused evanescent fields using conical lenses. *Opt. Express* 2010; 18(7): 7076.
- [26] Gu M, Kuriakose S, Gan X, A single beam near-field laser trap for optical stretching, folding and rotation of erythrocytes. *Opt. Express* 2007; 15(3): 1369.
- [27] Angelsky OV, Bekshaev AYa, Maksymyak PP, Maksymyak AP, and Hanson SG, Measurement of small light absorption in microparticles by means of optically induced rotation. *Opt. Express* 2015; 23(6): 7152–7163.
- [28] Angelsky OV, Maksymyak PP, Hanson S. *The Use of Optical-Correlation Techniques for Characterizing Scattering Object and Media*. SPIE Press PM71 Bellingham, USA; 1999.
- [29] Angelsky OV, Maksymyak PP. *Optical correlation diagnostics of surface roughness” in Optical Correlation Applications and Techniques*. SPIE Press, Bellingham; 2007.
- [30] Angelsky OV, Maksymyak PP. *Optical correlation diagnostics of surface roughness in coherent-domain optical methods*. In: Tuchin VV, editor. *Biomedical Diagnostics Environmental and Material Science*. Kluwer Academic Publishers; 2004.
- [31] Angelsky OV, Maksymyak PP, Polyansky VK, Measurement of refractive index of light scattering media (Avtorskoye svidetelstvo). 1986 (in Russian).
- [32] Punge A, Rizzoli SO, Jahn R, Wildanger J D, Meyer L, Schonle A,

Kastrup L, Hell SW, 3D reconstruction of high-resolution STED microscope images. *Microscopy Research and Technique* 2008; 71: 644–650.

[33] Vicidomini G, Bianchini P, Diaspro A, STED super-resolved microscopy. *Nat. Methods* 2018; 15: 173–182.

[34] Valle PJ, Fuentes A, Canales VF, Cagigas MA, Villo-Perez I, and Cagigal MP, Digital coronagraph algorithm. *OSA Continuum* 2018; 1(2): 625–633.

IntechOpen